The influence of short-term events on the hydrographic and biological structure of the southwestern Ross Sea

by

Randolph M. Jones*
Virginia Institute of Marine Science, College of William & Mary, Gloucester Pt., VA 23062;
email:rjones7@gmail.com

and

Walker O. Smith, Jr.
Virginia Institute of Marine Science, College of William & Mary, Gloucester Pt., VA 23062; email: wos@vims.edu

*: Corresponding author

Running Head: *Short-term Events in the Ross Sea*

Submitted to **Journal of Marine Systems**

December 27, 2015

Abstract

The Ross Sea continental shelf supports very high productivity and phytoplankton biomass. Conventional observational methods, including ship-based sampling, instrumented moorings, satellite imagery, and computer-based modelling, have illustrated the typical patterns of seasonal progression of the phytoplankton blooms. While spatial variability in the Ross Sea is known over relatively large scales, our understanding of smaller scales of variability (on the order of a few hours or several kilometers) is limited. Utilizing data from an autonomous glider, we examined the mechanisms driving both the transitions between stages of the phytoplankton bloom and the short-term perturbations in average chlorophyll concentrations. Three phases were defined: an accumulation phase, a dissipation period, and a post-dissipation phase. Short-term perturbations in chlorophyll were repeatedly observed and correlated with wind speed measured by a nearby weather station. Perturbations in chlorophyll were strongly influenced by the degree of temporal coupling between wind events and the depth of mixing, which varied among phases. Delays between wind events and chlorophyll changes of 12-24 h were observed during the accumulation phase, but shortened to 2-12 h following the transition to dissipation phase. Furthermore, while physical factors contributed to the observed short-term reductions in biomass and the appearance of chlorophyll at depth, we hypothesize that aggregate formation induced by turbulence led to rapid vertical flux. These results suggest that the small-scale, short-term physical perturbations may induce substantial vertical redistribution of biogenic material, which in turn can have significant biogeochemical impacts.

Keywords: mesoscale; Ross Sea, Antarctica; winds; chlorophyll; mixed layers

1. Introduction

The Ross Sea continental shelf is one of the most studied regions in the Southern Ocean, and has been characterized as being the most productive region in the Southern Ocean, contributing 28% of the total productivity (Arrigo et al., 1998b). Studies of the region have indicated the importance of this intense productivity and the substantial phytoplankton standing stocks in sustaining the food web (Smith et al., 2014). However, the substantial standing stocks of phytoplankton appear to be relatively spatially or temporally uncoupled from the distributions of middle and upper trophic level species (Ainley et al., 2015; Arrigo et al., 2000; Pinkerton and Bradford-Grieve, 2014). Furthermore, despite the substantial spatial variability observed (e.g., Arrigo and McClain 1994, Arrigo et al. 1999, Smith et al. 2013), the dominant scale of variability appears to be temporal (Smith et al., 2000). That is, temporal variations in chlorophyll ranges were up to 25 µg L^{-1} over two months, whereas variations in space tend at any single date to be far less extreme. Assessments of the variability at one location in the upper ocean, however, are rare. Smith et al. (2011a) collected data using *in situ* fluorometers at two locations and three depths, and demonstrated the degree of variability in chlorophyll during austral summer. Satellite climatologies also have indicated the temporal variations at single locations, although the satellite information is rarely available on a continuous basis due to frequent cloud cover.

In situ sampling has revealed a consistent temporal pattern in phytoplankton composition in the Ross Sea. In general the austral spring is dominated by the haptophyte *Phaeocystis antarctica* (Arrigo et al., 1999; Smith and Gordon, 1997). This species reaches very high biomass levels (up to 25 µg chlorophyll L^{-1}; Smith et al. 2003), but its biomass rapidly declines in late December and early January (Smith et al., 2014, 2011b, 2000), after which biomass of all phytoplankton groups generally remains low (Peloquin and Smith, 2007). Occasionally, a diverse assemblage of diatoms forms large blooms in late summer (Peloquin and Smith, 2007), the magnitude of which can be equal to those found in spring (Smith et al., 2011a). Although the magnitude of phytoplankton biomass varies among years, the temporal patterns have been corroborated by both satellite and in situ observations (Arrigo and McClain, 1994; Arrigo and Van Dijken, 2004; Arrigo and van Dijken, 2003; Arrigo et al., 2008; Smith and Comiso, 2008).

The major reasons for this observed seasonal bloom progression are believed to be both physical and biological. Beginning with bloom initiation in late October, the dominant controlling mechanisms are related to irradiance availability: decreasing ice coverage, seasonally increasing irradiance, lengthening photoperiods, and shoaling mixed layer depths (Smith and Gordon, 1997; Smith et al., 2000). Irradiance penetration through sea ice and snow cover is very low during spring and fall, with an attenuation of ~97% (Arrigo, 2014). Following rapid sea-ice retreat and moderate water column stabilization, phytoplankton productivity and biomass quickly increases, leading to large accumulations of particulate organic matter in the surface layer (Arrigo et al., 1998a; Smith and Gordon, 1997; Smith et al., 2000). A biomass maximum typically occurs in mid- to late December, and further growth is apparently limited by availability of the micronutrient iron (Sedwick et al., 2011, 2000). Overall, the temporal patterns in phytoplankton biomass result from changes in environmental conditions dictated by irradiance, vertical water column structure, and the degree of iron limitation (Arrigo et al., 1999; DiTullio and Smith, 1996; Peloquin and Smith, 2007; Sedwick et al., 2011).

The termination of the biomass maxima is largely thought to be the result of increased vertical flux of aggregated phytoplankton material, passive phytoplankton sinking (with rates enhanced due to nutrient stress), and losses resulting from grazing (Dunbar et al., 1998; Smith and Asper, 2001; Smith et al., 2011b, 2000). Smith et al. (2011b, 2000) demonstrated that two independent environmental factors created a temporal disconnect of ~30 days between the maxima of productivity and later biomass maxima in early January. Initially, limited iron availability leads to a reduction in phytoplankton production, with grazing and particle aggregation/sinking losses eventually becoming significant, thus leading to a reduction of biomass. Decreases in chlorophyll concentrations of 90% occur over a period of a few days (Smith et al., 2011a). However, the temporal progression of these seasonal changes in chlorophyll are disrupted by rapid "events" in which chlorophyll decreases over very short periods (hours) and recovers rapidly thereafter. Smith et al. (2011a) hypothesized that these were due to storms that altered surface stratification and diluted surface layers with low biomass water from depths, but provided no data on the physical forcing of such events. They also speculated that some events were the result of advection of low biomass waters, but again had no data to support this speculation.

This study investigated the temporal dynamics of a small region in the southern Ross Sea using a glider, an autonomous underwater vehicle that is propelled by buoyancy, which undulates from the surface to depth, and relays the data collected to a remote base station via satellite link (Eriksen et al., 2001). Gliders have recently been deployed in the Ross Sea, a region that has heavy ice cover and frequent storms, both of which restrict oceanographic sampling (Ainley et al., 2015; Kaufman et al., 2014; Queste et al., 2015). Gliders have slow speeds of < 0.25 m s^{-1} and typically cover horizontal distances of ~0.5-5 km $dive^{-1}$ or ~15-30 km d^{-1} (depending on the depth; Rudnick et al. 2004); as such, they are typically limited to resolving features with scales of a few days and a few km. Given that the spatial coverage of our glider was limited, the temporal variability over scales of months was assessed to elucidate the mechanisms that generate both the seasonal patterns as well as the short-term or "event scale" variations that commonly occur. We hypothesized that short-term variations in physical forcing had significant impacts on phytoplankton vertical distribution and potentially had important biogeochemical impacts on the entire southern Ross Sea.

2. Materials and Methods

A glider (iRobot Seaglider™ Model 1KA) was deployed from the fast ice near Cape Crozier, Ross Island (77.438°S, 169.746°E) on November 22, 2012 at 09:25 UTC (22:25 local time). It initially headed to the northeast for the first 50 dives before returning to the point of deployment. For the remainder of the study (dives 81-571), the glider followed a 'radiator' pattern (with three main latitudinal transects and several perpendicular, longitudinal transects; 25 km E/W x 50 km N/S), sampling multiple times along certain transects (Figure 1) and diving to approximately 800 m. The glider completed 571 dives over 78 d and was retrieved (76.771°S, 167.729°E) by the *RVIB Palmer* on February 8, 2013 at 00:44 UTC (13:44 local time). The glider was fitted with a SeaBird CT Sail, an Aanderaa Oxygen Optode 4330F, and Wet Labs ECO Triplet Puck. Data were collected approximately every 5 seconds; the Wet Labs ECO Puck was disabled below 250 m to conserve battery power. All data are available at http://www.bco-dmo.org/dataset/568868.

With the absence of ship-based support, glider calibration was limited to one CTD cast during recovery of the glider and water samples were collected at the ice edge during the glider deployment. The *RVIB Palmer* CTD profiles and water samples were used to calibrate glider temperature, salinity, and dissolved oxygen. Issues with the chlorophyll water samples obtained from the CTD profiles and ice edge led us to utilize a previous chlorophyll calibration for the fluorescence data (Kaufman et al., 2014). Hysteresis (the delay between measured and actual values at one depth) occurred through strong gradients in temperature, conductivity, and dissolved oxygen casts. Temperature and conductivity hysteresis were corrected by cross-calibration with the CTD profiles and application of a temporal offset. These corrections and other pre-analysis calculations were performed on the glider data set using the 'uea-seaglider-toolbox' developed by Dr. Bastien Queste (available at https://bitbucket.org/bastienqueste/uea-seaglider-toolbox/).

Glider fluorescence and particulate backscattering coefficients ($b_{bp}(\lambda)$, calculated from the glider optical backscattering counts; Stramski et al. 1998, 1999) were processed by regressing data from the final glider dive against *in situ* data (n=12). Samples for chlorophyll *a* were analyzed by fluorometry using the acid-addition method on a Turner Designs 10-AU fluorometer (JGOFS, 1996), and particulate matter concentrations were determined by filtering known volumes of seawater through combusted GFF filters, drying at 60°C, and pyrolysis on an elemental analyzer to obtain particulate organic carbon (POC) concentrations (Gardner et al., 2000). Fluorescence counts (FL) were converted into chlorophyll *a* concentrations (Chl) using the regression:

$$\text{Chl} = (\text{FL} + 141) * 0.00225;\ n = 12;\ R^2 = 0.94;\ p < 0.01$$

(Kaufman et al., 2014). To calculate $b_{bp}(\lambda)$, glider optical backscattering counts were converted to total volume scattering, β (117°, 470 nm) by subtracting dark counts and multiplying by a factory-calibrated scale factor, subtracting the volume scattering of seawater, β_w (Morel, 1974) from the total volume scattering to obtain volume scattering of particulates, β_p, and multiplying by $2\pi\chi$, where χ is 1.1 (Boss and Pegau, 2001). A regression based on the calibration cast:

$$\text{POC} = (42{,}850 * b_{bp}(470\ \text{nm})) + 57.47;\ n = 11;\ R^2 = 0.55;\ p < 0.01$$

was used to convert $b_{bp}(\lambda)$ into POC concentrations.

To prepare the calibrated, core data sets for analyses, individual glider dives were separated into their descending and ascending legs, with the deepest point in the dive marking the delineation between the two. With GPS positioning data available only when the glider was at the ocean surface, the GPS position obtained just prior to and just following a dive were interpolated to estimate GPS position data for that dive. A number of physical and biological parameters were derived for each cast. Values for sea surface temperature, salinity, and density were calculated by averaging observations from the top 5 m of the water column. Mixed layer depth (MLD) was computed using a potential density threshold method (Smith et al., 2013; Thomson and Fine, 2003), which defines the MLD as the minimum depth at which a 0.01 kg m^{-3} increase is observed over the density (σ_θ) at 3 m. Average integrated temperatures, densities, and chlorophyll concentrations were calculated using trapezoidal integration.

To investigate changes in the physical and biological variables through the seasonal progression of the phytoplankton bloom, temporal periods were identified using average 0-50 m chlorophyll glider data. Three periods, “accumulation”, “dissipation”, and “post-dissipation”, were defined which corresponded with biomass accumulation, biomass maintenance/decrease, and post-decrease, respectively. The accumulation period began when the glider entered into the radiator pattern on December 1 at 00:00 UTC and ended on December 14 at 00:00 UTC, approximately 12 h prior of the maximum average 0-50 m chlorophyll. The accumulation period spanned 13 d, and comprised 184 casts (casts 152-335). The dissipation period began December 14 at 00:00 UTC (approximately 12 h following the maximum average 0-50 m chlorophyll) and ended on January 7, 2013 at 00:00 UTC, 24 d later. The duration of this period is approximately twice as long as the accumulation period, as the bloom dissipates over a longer time. However, the definition of the period ending avoids extending into the period when biomass is no longer markedly decreasing (characteristic of the post-dissipation period). The dissipation period was comprised of 366 casts (glider casts 336-701). The post-dissipation period began January 7 at 00:00 UTC and ended 12 d later on January 19 at 00:00 UTC (casts 702-868; Table 1).

Hourly wind speeds were obtained from the Antarctic Meteorological Research Center (AMRC), University of Wisconsin, Madison (http://amrc.ssec.wisc.edu/). The AMRC-AWS is located east of Ross Island on the Ross Ice Shelf and is named Laurie II (77.451°S, 170.760°E; anemometer height approximately 40 m above sea level). It is located approximately 45 km from the center of the glider deployment (Figure 1).

Bootstrapped 95% confidence intervals of the means (n = 1000) were used to statistically compare variable averages between different temporal periods. Significant differences for pairwise comparisons were assessed at the $\alpha = 0.05$ level. To perform two-sample hypothesis tests on variability in the non-normal, autocorrelated glider, mooring, and wind speed time series, bootstrapped data for the temporal periods and variables of interest were fit to an autoregressive integrated moving average (ARIMA) model to obtain a ratio of residual variance. This process was repeated 1000 times to construct a 95% confidence interval for the ratio of residual variances. If the 95% confidence interval did not contain 1, the null hypothesis of equal variance between groups was rejected, and it was concluded that the variances differed. For the event-scale perturbation analyses and moving correlations, Pearson's linear correlation coefficients were calculated for glider and AWS variables. Correlation coefficients with p values ≤ 0.05 were considered statistically significant.

3. Results

Although spatial variability was noted within the small sampling region, the dominant mode of variability was temporal (Figure 2). The three defined periods – "accumulation", "dissipation", and "post-dissipation" – were based on changes in mean chlorophyll concentrations in the upper 50 m; specific events within each phase are discussed below. These mesoscale temporal variations were consistent with the general seasonal patterns in phytoplankton biomass, stratification, and temperature that had been repeatedly observed (Kaufman et al., 2014; Smith et al., 2014, 2000), but had marked short-term variations as part of the seasonal trends. That is, winds were variable throughout, and surface temperatures increased with time, with a modest decrease in mid- to late January. Mixed layer depths were also relatively constant, but like temperature increased slightly in the post-dissipation phase (Figure 2). Chlorophyll increased to a maximum on December 13 and decreased rapidly to levels approximately 25% of those found earlier (Figure 3). Particulate organic carbon concentrations also increased with time (Figure 3), and became maximal around December 25. POC decreased after that, but much more slowly than chlorophyll. As a result, POC:Chl ratios rose with time (Figure 3), as has been noted previously (Kaufman et al., 2014). The mean conditions and standard deviations found during the three periods for each variable are listed in Table 1.

Accumulation Phase

The accumulation phase was from December 1 – 14, and average chlorophyll levels increased from 3.8 to 6.2 µg L^{-1} (Figure 3). Within that period, one strong wind event that lasted 48-h (December 4-5) was observed (Figure 4). Other than this event, relatively calm conditions allowed MLDs to decrease and surface temperatures to increase. The stratification during these calm periods facilitated phytoplankton growth and accumulation, as demonstrated by the increased chlorophyll concentrations. A 12-24 h delay between the onset of the wind event and the initiation of a decrease in upper 30 m chlorophyll appeared to result from a delay in transferring the wind energy into changes to the upper water column structure (i.e., a MLD increase). During the accumulation period wind events typically began to affect mixed layer depths once wind speeds had nearly or fully reached the wind event's maximum velocity (Figure 4).

While wind events during the accumulation period were observed to affect chlorophyll after 12-24 h, changes to chlorophyll were observed almost immediately in response to changes to mixed layer depth. The December 4-5 wind event generated a MLD excursion from December 5-6 of 5-10 m to 60-80 m, which lasted for approximately 18 h. The initial responses in chlorophyll were limited to the upper 20 m of the water column and were observed from approximately noon until midnight UTC on December 4, 12 h prior to the onset of the MLD excursion. The deepening of the MLD started at 0000 UTC on December 5, and chlorophyll decreases were observed in the upper 40 m, and chlorophyll increases between 50 and 80 m.

Dissipation Phase

The dissipation phase was defined as beginning on December 14 (approximately 12 h following the maximum in the mean 0-50 m chlorophyll) and ending on January 7 (24 d). During this period chlorophyll concentrations were variable (ranging from 0.0 to 13.8 µg L^{-1}; Table 1), with several event-scale perturbations observed. A large reduction of chlorophyll from 6.5 to 1.9 µg L^{-1} and a re-establishment back to 5.8 µg L^{-1} over 4 d (December 14-18) was noted (Figure 3), but the phase also included several rapid event-scale perturbations (December 18-22) nearly equal in magnitude to the December 14-18 perturbation, but with greater vertical variations (Figure 5). A lack of strong wind events early in the phase (December 14-23) generated a MLD between 5 and 10 m and allowed chlorophyll to remain at approximately 70% of the seasonal maximum. Around December 23, there was a sharp reduction in average (0-50 m) chlorophyll, which coincided with the December 23-25 wind event and the resulting MLD-chlorophyll dissipation (Figure 5). As in the accumulation period, changes to chlorophyll were observed to coincide with the excursion of the MLD, which following the onset of the December 23-25 wind event, deepened to approximately 30 m for 12 h. It then further deepened to 40-75 m for 30 h as a successive wind event began. However, a reduction in chlorophyll had already begun in the surface 10 m around December 15, *prior* to any MLD excursions. Both the chlorophyll reductions prior to the change in MLD and the MLD increases resulted in the prominent reductions of chlorophyll between 10 and 30 m, and the appearance of chlorophyll between 40 and 100 m approximately 6-12 h before the onset of the MLD excursions on December 23. The subsequent wind event on December 25-27 and those following on December 29-30 continued to disrupt the MLDs, which resulted in a continuation of increased chlorophyll between 30 and 90 m during December 25-31 (Figure 5).

Post-dissipation Phase

The post-dissipation period had the least variability among all periods, and there are no large event-scale perturbations in chlorophyll during the phase. Three strong wind events occurred, as well as the beginning of a fourth prolonged, strong wind event that concluded following the end of the post-dissipation period (Figure 6). With low levels of chlorophyll in the upper 100 m following the effects of wind events and water column forcing on chlorophyll during the dissipation phase, the four post-dissipation wind events had a greatly reduced effect on chlorophyll vertical distribution. Chlorophyll was maintained at low levels in the upper 10 m; between 10 and 100 m chlorophyll decreased over the course of the phase (Figure 6).

Correlation Analysis

Overall variability (defined as residual variance) over the entire season was substantial, with marked variability in sea surface temperatures (SST), sea surface densities (SSD), and average 0-

50 m chlorophyll across the three periods. However, less variable wind speeds led to reduced variability in MLDs during the accumulation and post-dissipation periods. Variability in SST and SSD was greatest during the dissipation period, while variability in both wind speeds and MLDs generally decreased over the course of the three periods. Average 0-50 m chlorophyll variability was large and, like SST and SSD, had the greatest variability during the dissipation period. Finally, bootstrapped 95% confidence intervals of residual variance indicated that there were significant differences in variability between all combinations of SST, SSD, MLD, average 0-50 m chlorophyll, or wind speeds among the three phases (Jones, 2015). As the season progressed and chlorophyll began to dissipate throughout the upper 100 m, trends (such as the shift from increasing to decreasing chlorophyll and increased vertical fluxes) resulted in correlational shifts that were depth-dependent (Figure 7). While temperature and chlorophyll were strongly, positively correlated during the accumulation period when both were increasing and vertical flux was minimal, a moving correlation suggests a switch to a negative correlation ($r = -0.65$ to -0.41; $p<0.001$) in the upper 30 m around December 15-18 (Figure 8). Temperatures below 40 m during the dissipation remain significantly correlated with chlorophyll ($p<0.001$), with the correlations strengthening with depth (from $r = 0.28$ from 40-50 m to $r = 0.76$ from 80-90 m; Figure 7).

Shortly after the accumulation phase December 5 wind event, when wind speeds were low and MLDs had deepened in response to the winds, chlorophyll decreases were observed in the upper 30 m and chlorophyll increases were observed between 50 and 90 m. As a result, negative correlations between MLD and chlorophyll in the surface 40 m ($r = -0.43$ to -0.11; p = <0.001 to 0.046) and positive correlations between 50 and 80 m ($r = 0.12$ to 0.17; p = 0.002 to 0.038) were observed (Figure 7). Wind speeds were positively correlated with chlorophyll in the upper

30 m ($r = 0.21$ to 0.30; $p<0.001$), and were negatively correlated with chlorophyll between 40 and 100 m ($r = -0.51$ to -0.21; $p<0.001$).

During the dissipation period, correlation patterns over the upper 100 m between MLD and chlorophyll did not display a sign change, but did display a magnitude change, due to increased exchanges of chlorophyll (Figure 7). As in the accumulation period, changes to chlorophyll were observed to coincide with the excursions in the MLD. Correlations of MLD with chlorophyll between 10 and 30 m remained negative ($r = -0.26$ to -0.20; $p<0.001$), and between 40-100 m became more strongly positive ($r = 0.15$ to 0.49; $p<0.001$; Figure 7). The positive correlations during the accumulation period between wind speed and chlorophyll in the upper 30 m and negative correlations from 40 and 100 m reversed during the dissipation period, reflecting the increased temporal alignment (on the order of 2-12 h) between wind events and MLD-chlorophyll dissipations. As a result, wind speed and chlorophyll display a weak negative correlation from 10-20 m ($r = -0.15$; $p<0.001$), but positive correlations between 30 and 100 m ($r = 0.14$ to 0.40; $p<0.001$). Moving correlations suggest that the changes in correlation signs occurred on December 9-11, 2012, during the later stages of the accumulation period (Figure 8).

Period-wide trends during the post-dissipation phase (i.e., gradually increasing MLDs and decreasing chlorophyll) likely drive the negative correlations found between MLD and chlorophyll over the upper 100 m ($r = -0.36$ to -0.14; $p = <0.001$ to 0.019; Figure 7). The influence of trends were again highlighted between wind speed and chlorophyll by the shift from positive correlations between 30 and 100 m (weakly negative near the surface) during the dissipation phase to weak, negative correlations ($r = -0.31$ to -0.15; $p = <0.001$ to 0.019) across most of the water column (10-100 m) during the post-dissipation period. A shift in the correlation patterns between temperature and chlorophyll continued during the post-dissipation period, as chlorophyll reductions were observed over much of the upper 100 m and the warming trend continued (Figure 6). With that, negative correlations between temperature and surface chlorophyll deepened from 0-30 m to 10-60 m (r = −0.57 to −0.24; $p<0.001$) between the dissipation and post-dissipation periods (Figure 7). Also, the deeper, positive correlations between temperature and chlorophyll during dissipation (r = 0.28 to 0.76; $p<0.001$; 40-100 m) weakened and were limited to 90-100 m (r = 0.22; $p<0.001$). In the upper 10 m, temperature is positively correlated with chlorophyll (r = 0.27; $p<0.001$), indicating the influence of atmospheric forcing near the conclusion of the phytoplankton summer season (Figure 7). Lastly, moving correlations corroborate the depth dependent nature of these changes, with shifts from positive to negative correlation occurring later as depth increases (Figure 8).

4. Discussion

Biological and hydrographic conditions in the southwestern Ross Sea, as documented by glider observations and automatic weather station data, provided a broad view of the environmental conditions present and demonstrate the substantial spatial and temporal variability in the region. From our 2012-2013 glider observations, the surface waters were warmer, less dense, and experienced shallow MLDs when compared to other years (e.g., Smith et al. 2011a, Kaufman et al. 2014, Jones 2015, Queste et al. 2015). Wind data indicated that the 2012-2013 study period had low average wind speeds (Jones, 2015). Previous studies have demonstrated that the Ross Sea continental shelf has experienced decadal trends in increased ice concentrations, decreased open ice duration, and decreased salinities (Jacobs and Giulivi, 2010; Stammerjohn et al., 2008). Therefore, it is possible that a portion of the 2012-2013 seasonal trends may be partially attributable to the broader forcing observed across the entire Ross Sea sector.

It is well understood that environmental conditions in the Ross Sea exhibit high levels of spatial and temporal variability, as do phytoplankton concentrations as determined from ocean color observations and in situ measurements (Arrigo and McClain, 1994; Arrigo et al., 1999; Smith et al., 2013). In the Ross Sea, this variability may be caused by factors such as ice, vertical or horizontal advection, stratification, and seasonality. Our observations, collected within a small area (25x50 km), were characterized by 1) relatively pronounced mesoscale variability, 2) perturbations in water column variables during and subsequent to wind events, 3) a decreasing seasonal trend in time from the dissipation to post-dissipation periods when compared to previous studies using gliders (Kaufman et al., 2014; Queste et al., 2015), and 4) movement of chlorophyll to depth that was related to wind mixing events. The variability observed reflects different environmental factors. For example, differences in the proximity to ice between different study locations may have had an effect on the observed differences in variability. Our glider operated close to a pack ice, which especially during the accumulation and dissipation periods may have facilitated the rapid excursions in chlorophyll. Ice can add a great deal of variability to the vertical stratification and irradiance availability of a water column, as melting ice imparts low salinity water at the surface, changing stratification, which in turn leads to variability in phytoplankton growth.

During the accumulation period short-term disturbances to water column structure driven by wind events had the greatest effect on chlorophyll. Changes resulting from wind mixing typically propagated from the surface to depth and were determined by the speed and duration of a wind event. Wind mixing events changed mixed layer depths as well as the temperature and density vertical profiles in the upper 100 m. For example, wind events on December 4-5 and two wind events from December 23-26 (durations of ~48-96 h) resulted in MLD increases from ~5-

10 m to ~25-80 m, where they remained for approximately 36-72 h (slightly shorter than wind events and with a lag; Figures 4, 5). Mixing was also indicated by temperature changes during periods of increased MLDs, where noticeable increases in temperature were observed between 30 and 90 m during the December 23-26 mixing event. Deeper MLDs (60-80 m) were required to increase temperatures between 70 and 90 m (Figures 4,5). In contrast, relatively calm periods, such as those observed over the first two days of December and at the end of the accumulation period, promoted the shoaling of MLDs to less than 15 m (Figure 4). By limiting deep mixing and maintaining phytoplankton in the well-lit, presumably nutrient-replete surface layer, shallow and stable MLDs generate periods (hours to days) that allow biomass to accumulate and growth to proceed under irradiance-saturated conditions (Smith and Donaldson, 2015).

The delays between the onset of a wind event and the resulting changes to the mixed layer during the accumulation period were on the order of 12-24 h (Figure 4). Therefore, the temporal alignment of accumulated biomass (following calm, shallow MLD periods) and the deepening of MLDs (in response to wind energy inputs) produced significant correlations in the upper 30 m between wind speed or MLD with chlorophyll ($r = 0.21$ to 0.30 and $r = -0.43$ to -0.35, respectively; $p<0.001$; Figure 7). However, between 40 and 100 m, these correlations switched signs and magnitudes, with wind speed and chlorophyll negatively correlated ($r = -0.51$ to -0.21; $p<0.001$) and MLD and chlorophyll positively correlated between 50 and 80 m ($r = 0.12$ to 0.17; $p = 0.011$ to 0.002; Figure 7).

The contrasting observations of the correlations between wind speed and MLD with chlorophyll, and the change in correlational sign that occurs at the inflection point at 40 m, are both the result two inter-related processes. First, the temporal uncoupling between a wind event and the resultant mixing response or MLD excursion (ca. 12-24 h) leads to the differences in signs between wind speed and MLD correlations. Importantly, the timing between MLD excursions and chlorophyll responses experience little to no change, thus maintaining the relationship of MLD with chlorophyll between the accumulation and the dissipation period. Second, the resultant mixing effects of the wind event (and increased MLDs) have depth-dependent influences on chlorophyll. Chlorophyll is reduced in shallow waters and appears in deeper waters as a result of the MLD excursions to depth with little delay. During the accumulation period and the December 5-7 wind event, biomass increased substantially between 40 and 80 m following the wind event (Figure 4), which is unlikely to be fully explained solely by wind induced mixing and MLD excursions, due to the relatively shallow effects of wind mixing (MLDs increasing to 25-80 m). The timing and nature of the disappearance of chlorophyll shallower than 40 to 50 m and the appearance of chlorophyll between 50 and 90 m suggests that wind-induced mixing caused aggregate formation and enhanced vertical flux (Burd and Jackson, 2009; Waniek, 2003). That is, particle-particle interaction was enhanced by turbulence, and resulted in the formation of larger particles (or aggregates) that had significant numbers of chlorophyll-containing cells. These larger particles sank rapidly and were then observed at depth. For example, chlorophyll disappearances between 0 and 30 m preceded the MLD increases and are aligned temporally with the maximal wind speeds on December 4, 2012. Within 12 h, biomass appeared at 70 to 90 m prior to the influence of the MLD at those depths (Figure 4). Together, this suggests that vertical biomass displacement may be explained by vertical water movement (the result of wind/MLD events), coupled with aggregate formation and vertical flux (the result of wind derived turbulence).

The overall abundance of aggregates is a function of production and loss processes that are influenced by several environmental factors, such as particle stickiness and frequency of particle interaction (Burd and Jackson, 2009). Depending on the complex interplay of these factors, aggregate formation and increased particle sizes may develop. Alternatively, wind-driven turbulence may also cause aggregate or particle disruption, where smaller particles may slow the rates of vertical fluxes and the movement of biomass to depth. Coincident with slower sinking rates, increased remineralization of smaller particles might also occur. However, our data suggest that the net processes during these short intervals resulted in increased aggregate sizes and enhanced vertical flux of chlorophyll to depth.

The majority of biomass reductions in the surface waters and rapid appearances in waters deeper than 40-50 m occurred during the dissipation period. Biomass during this time is typically dominated by *Phaeocystis antarctica* (Arrigo et al., 1999; Smith and Gordon, 1997; Smith et al., 2013), and it has been suggested that the colonial form of *Phaeocystis* contributes greatly to aggregate formation and subsequent, rapid vertical flux to depth (DiTullio et al., 2000; Smith and Asper, 2001; Smith et al., 2011b). With differences in the carbon to chlorophyll ratios between *Phaeocystis* and diatom species (Kaufman et al., 2014), observations of POC:Chl during the study periods suggest low POC:Chl ratios were present (*Phaeocystis*-dominated blooms; Kaufman et al. 2014) during the accumulation and dissipation periods (Figure 3). Therefore, it is likely that aggregate processes on *Phaeocystis*-dominated blooms during the dissipation period likely played a role in the enhanced vertical flux to depth.

As biomass became maximal and the bloom entered the dissipation period, changes in wind speeds, MLDs, and chlorophyll caused shifts in the correlations among those variables. The most altered correlation (Figure 7) was between wind speed and chlorophyll, with a negative correlation between 10 and 20 m ($r = -0.15$; $p<0.001$) and positive correlations between 30 and 100 m ($r = 0.14$ to 0.40; $p<0.001$). This reflects a change in the delay from 12-24 h during the accumulation period to 2-12 h during the dissipation period between the onset of a wind event and the resulting response in the MLD. This is illustrated by the prominent wind events during the dissipation period. Following a calm period from December 14-22 with variable and high chlorophyll levels in the upper 40 m, wind events from December 23-27 quickly reduced average chlorophyll concentrations from 4 - 8 to 1.5 - 3 μg L^{-1} (Figure 3). With the stronger temporal coupling between wind events and a response in MLD, the effect of the increased winds on chlorophyll was rapid. Compared with the accumulation phase, the dissipation correlations suggest that wind events typically cause chlorophyll to be removed from surface waters (shallower than 20-40 m) and appear between 50 and 100 m (Figure 5). Moving correlation analyses suggest that this shift in the signs of the wind speed with chlorophyll correlations occurred just prior to the bloom maxima (December 9-13; Figure 8).

While the correlations between wind speed and chlorophyll changed from the accumulation to the dissipation period due to changes in timing, there are minimal changes for the correlations between MLD and chlorophyll moving into the dissipation period, as changes in chlorophyll remain tightly coupled to MLD. Significant, negative correlations near the surface weakened (10 to 30 m; $r = -0.26$ to -0.20; $p<0.001$), while significant correlations at depth strengthened (40 to 100 m; $r = 0.15$ to 0.49; $p<0.001$; Figure 7). Generally, the underlying mechanism of shoaled MLDs encouraging biomass buildup and minimal mixing to depth, and increased MLDs allowing deeper mixing to carry phytoplankton biomass to depths and stimulate aggregate formation appears to hold from the accumulation through the dissipation period, leaving the correlation pattern largely intact. During the dissipation period, this pattern is most apparent during the MLD excursions from 5-10 m to 70-75 m that occurred on December 23-26. The decline of chlorophyll between 10 and 40 m on December 22 results in chlorophyll appearances between 50 and 90 m (Figure 5).

As illustrated by a period of low wind speeds and stable, shallow MLDs (December 14-22), the coupling of wind events and MLD excursions with chlorophyll changes may not always be the case when noting the variability in chlorophyll observed between 10 and 50 m. Nevertheless, while little change is noted in MLDs during this low wind period, a short duration (8-12 h) increase in wind speed on December 18 appears to have an effect on chlorophyll and drive chlorophyll reductions in shallow waters (10-20 m) and its appearance at depth (30-50 m) occurring on December 19 (Figure 5).

By the post-dissipation period (January 7-19), reductions of chlorophyll across the upper 100 m caused the correlations of wind speed and MLD with chlorophyll to weaken. That is, with chlorophyll biomass largely at post-bloom levels, three wind events (January 10, 12-13, and 14-15) and limited MLD excursions have a minimal effect upon chlorophyll vertical distribution (Figure 6). With the end of the growing season approaching (Smith et al., 2011a), trends of increasing wind events, the associated deepening of the MLD, and decreasing chlorophyll appear to be the driving factors in a switch to negative correlations for both wind speed and MLD (Figure 7).

Among several factors that may lead to variability in shallow chlorophyll, these observations suggest strongly that vertical stratification may play one of the greater roles in influencing the variability observed in the upper 100 m of the water column. Observations of seasonal changes to the temporal coupling between wind events and MLD excursions illustrate that alternating calm and perturbation periods rework vertical stratification, so that mid-season wind events are more effective at rapidly deepening mixing and transferring chlorophyll to depth (Smith and

Jones, 2015). Lastly, changes to the temporal coupling between wind events and MLD excursions may be due to the shifting wind direction over the course of the accumulation and dissipation periods. Wind directions during the accumulation period are typically from the southwest with an average direction of 222°. From the early through the late dissipation period, the wind direction shifts to the south and eventually to the east-southeast with an average direction of 167°. The shift is likely due to seasonal changes in regional atmospheric circulation patterns as influenced by the local topography (Ross Island and Ross Ice Shelf; Dinniman et al. 2007).

5. Conclusions

The seasonal progression in surface layer hydrography and biological conditions is influenced by short-term events driven by winds. Wind energy is transferred to the water column, increasing turbulence and in most cases mixed layer depths. These in turn alter vertical chlorophyll distributions throughout the water column by enhancing particle-particle interactions, generating larger aggregates which sink more rapidly to depth. Such events and changes are generally short (less than 2 days) and are interspersed with periods of low winds and strong stratification that promote rapid phytoplankton growth. The coupling of the wind-stratification-chlorophyll linkage depends on the season, and is greatest when biomass is near maximum and least when biomass is increasing or has largely dissipated. These event-scale perturbations impose substantial variability on the seasonal pattern and have the potential for altering vertical distributions of organic matter and its flux to depth.

Acknowledgements. This work was supported by a National Science Foundation grant (ANT 1142174 to WOS). Logistic support was provided by the United States Antarctic Program, Raytheon Polar Services, and the *RVIB Nathaniel B. Palmer*. We thank David Ainley, Vernon Asper, and Kevin Martin for programmatic guidance and glider support. This is VIMS contribution number XXXX.

References Cited

Ainley, D.G., Ballard, G., Jones, R.M., Jongsomjit, D., Pierce, S.D., Smith, W.O., Veloz, S., 2015. Trophic cascades in the western Ross Sea, Antarctica: revisited. Marine Ecology Progress Series 534, 1–16. doi:10.3354/meps11394

Arrigo, K.R., 2014. Sea ice ecosystems. Annual Review of Marine Science 6, 439–67. doi:10.1146/annurev-marine-010213-135103

Arrigo, K.R., DiTullio, G.R., Dunbar, R.B., Robinson, D.H., Van Woert, M.L., Worthen, D.L., Lizotte, M.P., 2000. Phytoplankton taxonomic variability in nutrient utilization and primary production in the Ross Sea. Journal of Geophysical Research 105, 8827–8846.

Arrigo, K.R., McClain, C.R., 1994. Spring phytoplankton production in the western Ross Sea. Science 266, 261–263. doi:10.1126/science.266.5183.261

Arrigo, K.R., Robinson, D.H., Worthen, D.L., Dunbar, R.B., DiTullio, G.R., Van Woert, M.L., Lizotte, M.P., 1999. Phytoplankton community structure and the drawdown of nutrients and CO_2 in the Southern Ocean. Science 283, 365–367. doi:10.1126/science.283.5400.365

Arrigo, K.R., van Dijken, G.L., 2003. Phytoplankton dynamics within 37 Antarctic coastal polynya systems. Journal of Geophysical Research 108, 3271. doi:10.1029/2002JC001739

Arrigo, K.R., Van Dijken, G.L., 2004. Annual changes in sea-ice, chlorophyll a, and primary production in the Ross Sea, Antarctica. Deep-Sea Research II 51, 117–138. doi:10.1016/j.dsr2.2003.04.003

Arrigo, K.R., van Dijken, G.L., Bushinsky, S., 2008. Primary production in the Southern Ocean, 1997-2006. Journal of Geophysical Research 113, C08004. doi:10.1029/2007JC004551

Arrigo, K.R., Weiss, A.M., Smith, W.O., 1998a. Physical forcing of phytoplankton dynamics in the southwestern Ross Sea. Journal of Geophysical Research 103, 1007–1021.

Arrigo, K.R., Worthen, D.L., Schnell, A., Lizotte, M.P., 1998b. Primary production in Southern Ocean waters. Journal of Geophysical Research 103, 15587–15600.

Boss, E.S., Pegau, W.S., 2001. Relationship of light scattering at an angle in the backward direction to the backscattering coefficient. Applied Optics 40, 5503–5507.

Burd, A.B., Jackson, G.A., 2009. Particle aggregation. Annual Review of Marine Science 1, 65–90. doi:10.1146/annurev.marine.010908.163904

Dinniman, M.S., Klinck, J.M., Smith, W.O., 2007. Influence of sea ice cover and icebergs on circulation and water mass formation in a numerical circulation model of the Ross Sea, Antarctica. Journal of Geophysical Research 112, C11013. doi:10.1029/2006JC004036

DiTullio, G.R., Grebmeier, J.M., Arrigo, K.R., Lizotte, M.P., Robinson, D.H., Leventer, A.R., Barry, J.P., Van Woert, M.L., Dunbar, R.B., 2000. Rapid and early export of *Phaeocystis antarctica* blooms in the Ross Sea, Antarctica. Nature 404, 595–598. doi:10.1038/35007061

DiTullio, G.R., Smith, W.O., 1996. Spatial patterns in phytoplankton biomass and pigment distributions in the Ross Sea. Journal of Geophysical Research 101, 18467–18477. doi:10.1029/96JC00034

Dunbar, R.B., Leventer, A.R., Mucciarone, D.A., 1998. Water column sediment fluxes in the Ross Sea, Antarctica: Atmospheric and sea ice forcing. Journal of Geophysical Research 103, 30741–30759. doi:10.1029/1998JC900001

Eriksen, C.C., Osse, T.J., Light, R.D., Wen, T., Lehman, T.W., Sabin, P.L., Ballard, J.W., Chiodi, A.M., 2001. Seaglider: a long-range autonomous underwater vehicle for oceanographic research. IEEE Journal of Oceanic Engineering 26, 424–436. doi:10.1109/48.972073

Gardner, W.D., Richardson, M.J., Smith, W.O., 2000. Seasonal patterns of water column particulate organic carbon and fluxes in the Ross Sea, Antarctica. Deep-Sea Research II 47, 3423–3449.

Jacobs, S.S., Giulivi, C.F., 2010. Large multidecadal salinity trends near the Pacific–Antarctic continental margin. Journal of Climate 23, 4508–4524. doi:10.1175/2010JCLI3284.1

JGOFS, 1996. Protocols for the Joint Global Ocean Flux Study (JGOFS) Core Measurements, IOC SCOR Rpt. 19. Bergen, Norway.

Jones, R.M., 2015. The Influence of Short-Term Events on the Hydrographic and Biological Structure of the Southwestern Ross Sea. The College of William and Mary.

Kaufman, D.E., Friedrichs, M.A.M., Smith, W.O., Queste, B.Y., Heywood, K.J., 2014. Biogeochemical variability in the southern Ross Sea as observed by a glider deployment. Deep-Sea Research I 92, 93–106.

Morel, A., 1974. Optical properties of pure water and pure sea water, in: Jerlov, N.G., Nielsen, E.S. (Eds.), Optical Aspects of Oceanography. Elsevier, New York, pp. 1–24.

Peloquin, J.A., Smith, W.O., 2007. Phytoplankton blooms in the Ross Sea, Antarctica: Interannual variability in magnitude, temporal patterns, and composition. Journal of Geophysical Research 112, C08013. doi:10.1029/2006JC003816

Pinkerton, M.H., Bradford-Grieve, J.M., 2014. Characterizing foodweb structure to identify potential ecosystem effects of fishing in the Ross Sea, Antarctica. ICES Journal of Marine Science 71, 1542–1553.

Queste, B.Y., Heywood, K.J., Smith, W.O., Kaufman, D.E., Jickells, T.D., Dinniman, M.S., 2015. Observations of dissolved oxygen dynamics during a phytoplankton bloom in the Ross Sea polynya. Antarctic Science 27, 362–372. doi:10.1017/S0954102014000881

Rudnick, D.L., Davis, R.E., Eriksen, C.C., Fratantoni, D.M., Perry, M.J., 2004. Underwater gliders for ocean research. Marine Technology Society Journal 38, 73–84. doi:10.4031/002533204787522703

Sedwick, P.N., DiTullio, G.R., Mackey, D.J., 2000. Iron and manganese in the Ross Sea, Antarctica: Seasonal iron limitation in Antarctic shelf waters. Journal of Geophysical Research 105, 11321–11336. doi:10.1029/2000JC000256

Sedwick, P.N., Marsay, C.M., Sohst, B.M., Aguilar-Islas, A.M., Lohan, M.C., Long, M.C., Arrigo, K.R., Dunbar, R.B., Saito, M.A., Smith, W.O., DiTullio, G.R., 2011. Early season depletion of dissolved iron in the Ross Sea polynya: Implications for iron dynamics on the Antarctic continental shelf. Journal of Geophysical Research 116, 1–19. doi:10.1029/2010JC006553

Smith, W.O., Ainley, D.G., Arrigo, K.R., Dinniman, M.S., 2014. The oceanography and ecology of the Ross Sea. Annual Review of Marine Science 6, 469–487. doi:10.1146/annurev-marine-010213-135114

Smith, W.O., Asper, V.L., 2001. The influence of phytoplankton assemblage composition on biogeochemical characteristics and cycles in the southern Ross Sea, Antarctica. Deep-Sea Research I 48, 137–161. doi:10.1016/S0967-0637(00)00045-5

Smith, W.O., Asper, V.L., Tozzi, S., Liu, X., Stammerjohn, S.E., 2011a. Surface layer variability in the Ross Sea, Antarctica as assessed by in situ fluorescence measurements. Progress in Oceanography 88, 28–45. doi:10.1016/j.pocean.2010.08.002

Smith, W.O., Comiso, J.C., 2008. Influence of sea ice on primary production in the Southern Ocean: A satellite perspective. Journal of Geophysical Research 113, C05S93. doi:10.1029/2007JC004251

Smith, W.O., Dennett, M.R., Mathot, S., Caron, D.A., 2003. The temporal dynamics of the flagellated and colonial stages of *Phaeocystis antarctica* in the Ross Sea. Deep-Sea Research II 50, 605–617. doi:10.1016/S0967-0645(02)00586-6

Smith, W.O., Donaldson, K., 2015. Photosynthesis–irradiance responses in the Ross Sea, Antarctica: a meta-analysis. Biogeosciences 12, 3567–3577. doi:10.5194/bg-12-3567-2015

Smith, W.O., Gordon, L.I., 1997. Hyperproductivity of the Ross Sea (Antarctica) polynya during austral spring. Geophysical Research Letters 24, 233–236. doi:10.1029/96GL03926

Smith, W.O., Jones, R.M., 2015. Vertical mixing, critical depths, and phytoplankton growth in the Ross Sea. ICES Journal of Marine Science 72, 1952–1960. doi:10.1093/icesjms/fsu234

Smith, W.O., Marra, J., Hiscock, M.R., Barber, R.T., 2000. The seasonal cycle of phytoplankton biomass and primary productivity in the Ross Sea, Antarctica. Deep-Sea Research II 47, 3119–3140.

Smith, W.O., Shields, A.R., Dreyer, J.C., Peloquin, J.A., Asper, V.L., 2011b. Interannual variability in vertical export in the Ross Sea: Magnitude, composition, and environmental correlates. Deep-Sea Research I 58, 147–159. doi:10.1016/j.dsr.2010.11.007

Smith, W.O., Tozzi, S., Long, M.C., Sedwick, P.N., Peloquin, J.A., Dunbar, R.B., Hutchins, D.A., Kolber, Z., DiTullio, G.R., 2013. Spatial and temporal variations in variable fluoresence in the Ross Sea (Antarctica): Oceanographic correlates and bloom dynamics. Deep-Sea Research I 79, 141–155. doi:10.1016/j.dsr.2013.05.002

Stammerjohn, S.E., Martinson, D.G., Smith, R.C., Yuan, X., Rind, D., 2008. Trends in Antarctic annual sea ice retreat and advance and their relation to El Niño–Southern Oscillation and Southern Annular Mode variability. Journal of Geophysical Research 113, C03S90. doi:10.1029/2007JC004269

Stramski, D., Reynolds, R.A., Kahru, M., Mitchell, B.G., 1999. Estimation of particulate organic carbon in the ocean from satellite remote sensing. Science 285, 239–242. doi:10.1126/science.285.5425.239

Stramski, D., Reynolds, R.A., Mitchell, B.G., 1998. Relationships between the backscattering coefficient, beam attenuation coefficient and particulate organic matter concentrations in the Ross Sea, in: Ackleson, S., Cambell, J. (Eds.), Proceedings of Ocean Optics. Kona, Hawaii, pp. 1–10.

Thomson, R.E., Fine, I. V., 2003. Estimating mixed layer depth from oceanic profile data. Journal of Atmospheric and Oceanic Technology 20, 319–329.

Waniek, J.J., 2003. The role of physical forcing in initiation of spring blooms in the northeast Atlantic. Journal of Marine Systems 39, 57–82. doi:10.1016/S0924-7963(02)00248-8

Table 1. Mean and standard deviations of conditions measured during the three phases within the seasonal progression of hydrographic and biological variables. Numbers in brackets are the ranges encountered. SST = sea surface temperature; SSS = sea surface salinity; SSD = sea surface density.

Variable/Phase	**Accumulation**	**Dissipation**	**Post-Dissipation**
Wind Speed [m s^{-1}]	4.1 ± 3.3 [0.0 to 16.6]	3.8 ± 3.0 [0.0 to 13.8]	3.2 ± 2.6 [0.0 to 12.1]
SST [˚C]	−1.14 ± 0.22 [−1.74 to −0.22]	−0.04 ± 0.58 [−1.31 to 1.43]	0.70 ± 0.43 [−0.54 to 2.00]
SSS	34.409 ± 0.104 [33.690 to 34.632]	34.131 ± 0.245 [33.310 to 34.460]	34.222 ± 0.101 [33.824 to 34.400]
SSD [kg m^{-3}]	27.687 ± 0.086 [27.109 to 27.842]	27. 408 ± 0.212 [26.526 to 27.727]	27.442 ± 0.097 [27.030 to 27.612]
Mixed layer depth [m]	21.7 ± 24.9 [3.1 to 166.4]	16.3 ± 18.1 [3.0 to 91.8]	13.4 ± 7.7 [3.5 to 44.3]
Chlorophyll [μg L^{-1}]*	4.79 ± 1.14 [2.55 to 7.08]	3.34 ± 1.16 [1.28 to 7.50]	1.12 ± 0.33 [0.58 to 2.12]

*: Average for upper 50 m

Figure Legends

Figure 1. Map depicting the study location and glider track in the southern Ross Sea. Red square in insert indicates the study area.

Figure 2. Temporal variations in a) wind speeds, b) sea surface temperatures (SST), c) mixed layer depths (MLD) over the entire study period. Dashed lines indicate the delineation of accumulation, dissipation and post-dissipation periods.

Figure 3. Temporal variations in a) average 0-50 m particulate organic carbon (POC) concentrations, b) average 0-50 m chlorophyll (Chl) concentrations, and c) the ratio of POC to chlorophyll over the entire study period. Dashed lines delineate the accumulation, dissipation and post-dissipation periods.

Figure 4. Temporal changes within the accumulation period in a) wind speeds and mixed layer depths (MLD), and average chlorophyll concentrations (Chl) and temperatures (T) from b) 0-10 m, c) 10-20 m, d) 20-30 m, e) 30-40 m, f) 50-60 m, g) 70-80 m, and h) 90-100 m.

Figure 5. Temporal changes within the dissipation period in a) wind speeds and mixed layer depths (MLD), and average chlorophyll concentrations (Chl) and temperatures (T) from b) 0-10 m, c) 10-20 m, d) 20-30 m, e) 30-40 m, f) 50-60 m, g) 70-80 m, and h) 90-100 m.

Figure 6. Temporal changes within the post-dissipation period in a) wind speeds and mixed layer depths (MLD), and average chlorophyll (Chl) concentrations and temperatures (T) from b) 0-10 m, c) 10-20 m, d) 20-30 m, e) 30-40 m, f) 50-60 m, g) 70-80 m, and h) 90-100 m.

Figure 7. Pearson product-moment correlation coefficients between wind speed and average 10 m binned chlorophyll during the a) accumulation, b) dissipation, and c) post-dissipation periods, between mixed layer depth and 10 m binned chlorophyll during the d) accumulation, e) dissipation, and f) post-dissipation periods, and between 10 m binned temperature and chlorophyll during the g) accumulation, h) dissipation, and i) post-dissipation periods. Asterisks indicate significance at the $p < 0.05$ level.

Figure 8. Moving correlations utilizing a moving window of 7 days between a) 0-10 m, b) 10-20 m, c) 20-30 m, d) 30-40 m, e) 50-60 m, f) 70-80 m, and g) 90-100 m average 10 m binned chlorophyll with wind speed (blue lines), mixed layer depth (MLD; red lines), and the corresponding 10 m binned temperature average (Temp; black lines). Data are aligned on the x-axis at the window center.

Fig. 1

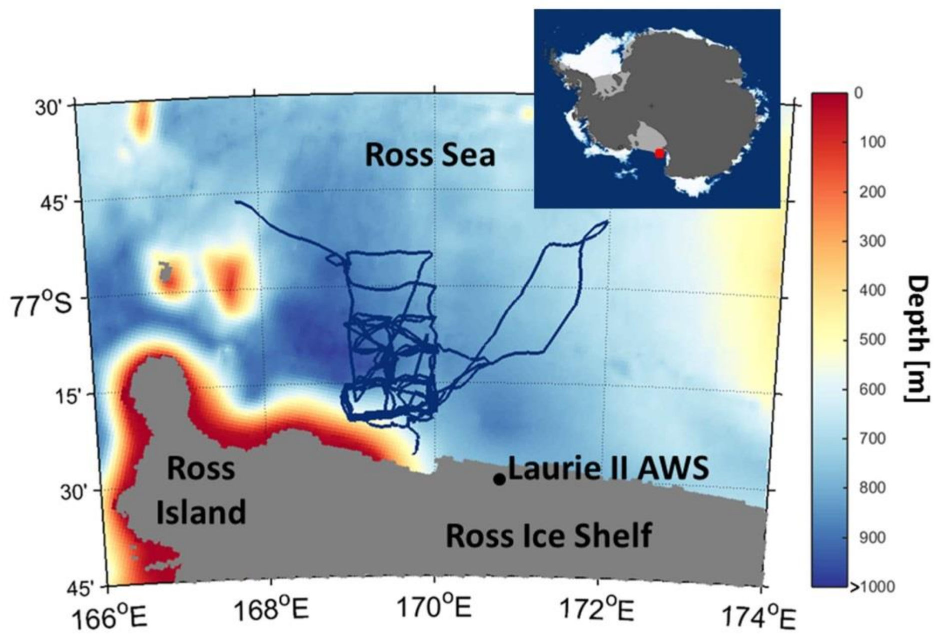
Ross Sea
Ross Island
Laurie II AWS
Ross Ice Shelf
30'
45'
77°S
15'
30'
45'
166°E
168°E
170°E
172°E
174°E
Depth [m]
0
100
200
300
400
500
600
700
800
900
>1000

Fig. 2

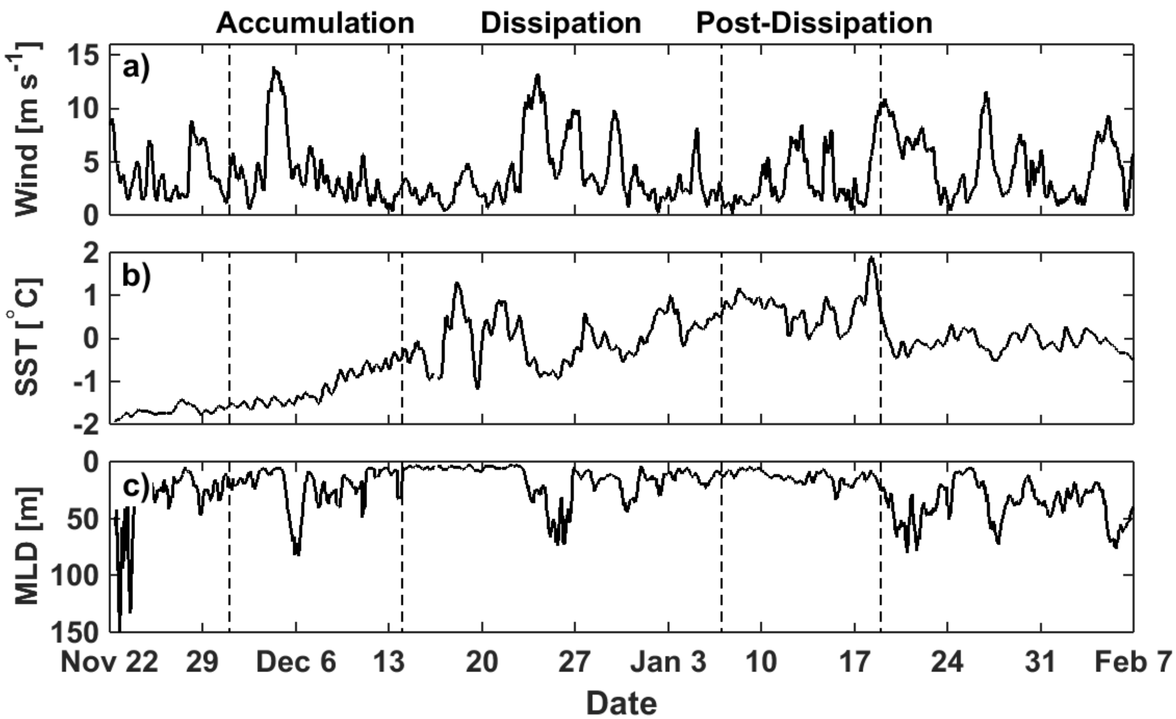
Accumulation
Dissipation
Post-Dissipation
a)
Wind [m s-1]
15
10
5
0
b)
SST [°C]
2
1
0
-1
-2
c)
MLD [m]
0
50
100
150
Nov 22
29
Dec 6
13
20
27
Jan 3
10
17
24
31
Feb 7
Date

Fig. 3.

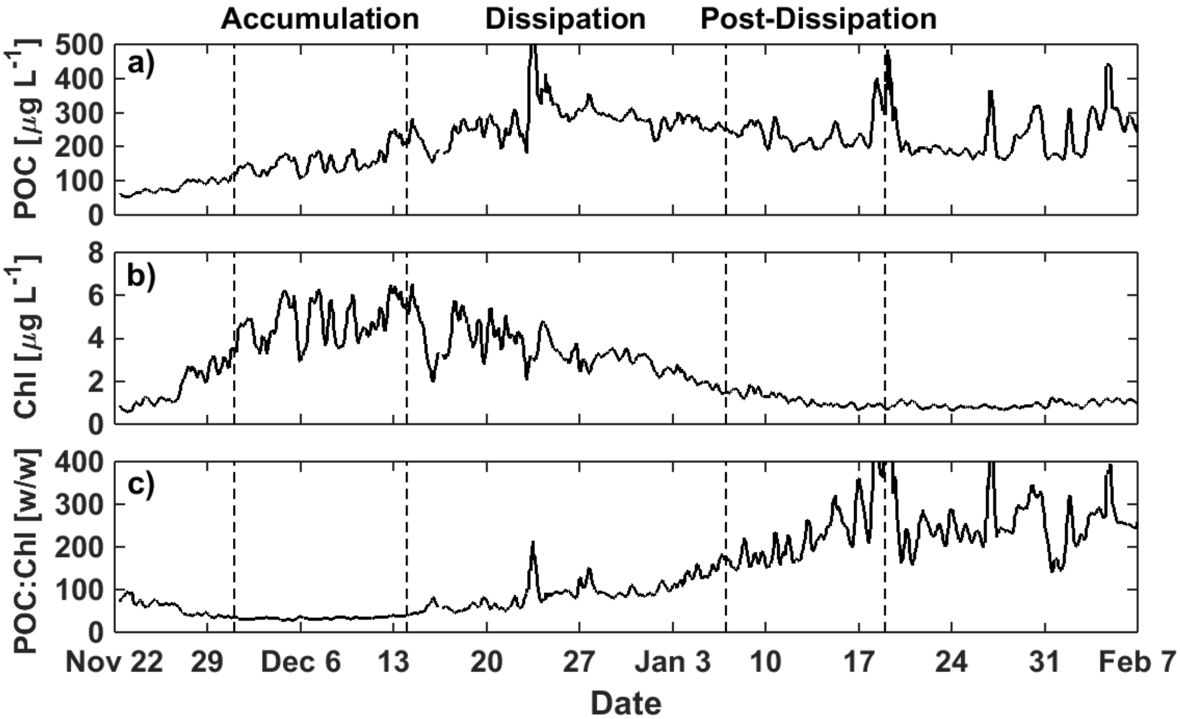
Accumulation
Dissipation
Post-Dissipation
a)
POC [μg L^{-1}]
500
400
300
200
100
0
b)
Chl [μg L^{-1}]
8
6
4
2
0
c)
POC:Chl [w/w]
400
300
200
100
0
Nov 22
29
Dec 6
13
20
27
Jan 3
10
17
24
31
Feb 7
Date

Fig. 4

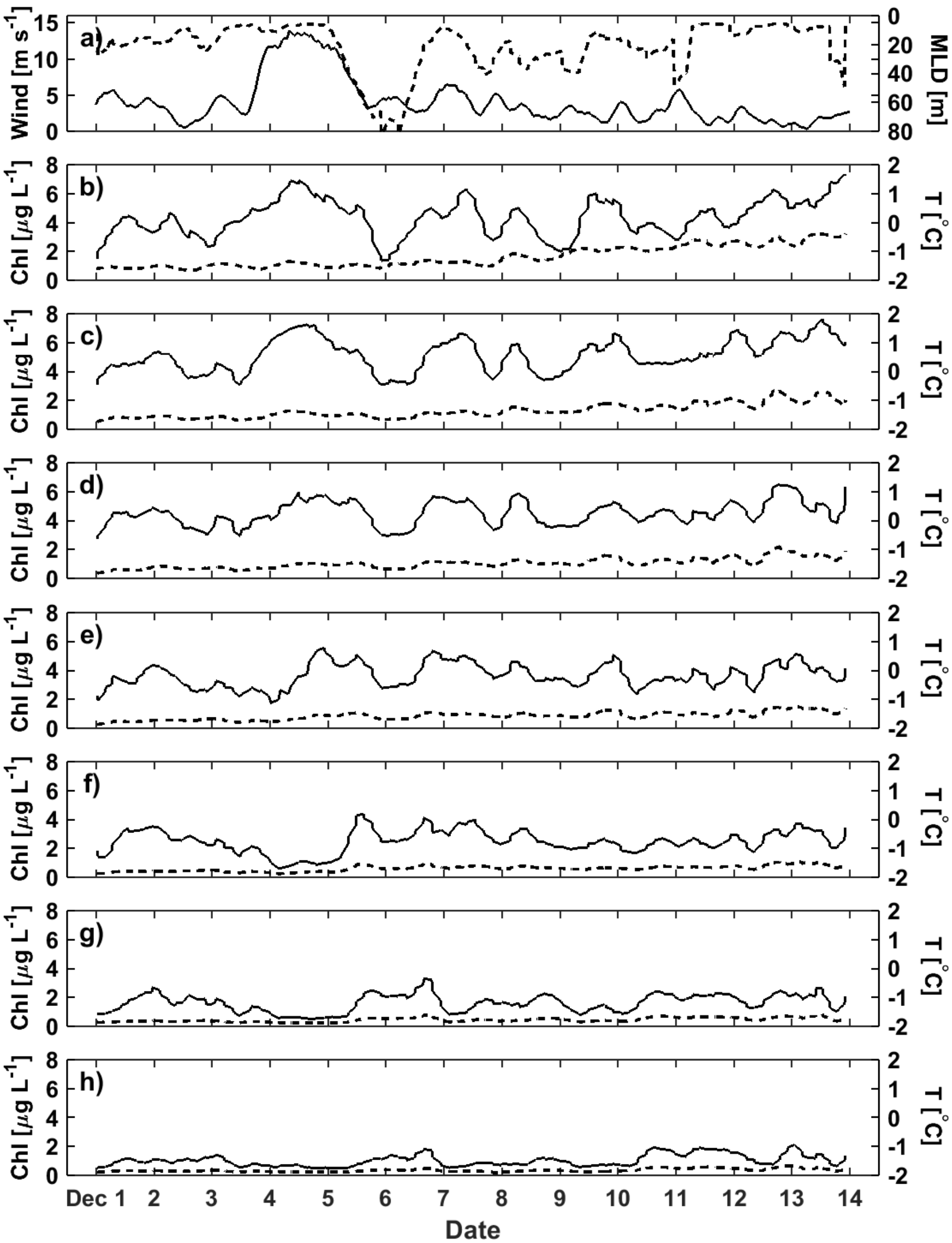
Wind [m s^{-1}]
MLD [m]
Chl [μg L^{-1}]
T [$^{\circ}$C]
a)
b)
c)
d)
e)
f)
g)
h)
Dec 1 2 3 4 5 6 7 8 9 10 11 12 13 14
Date

Fig. 5

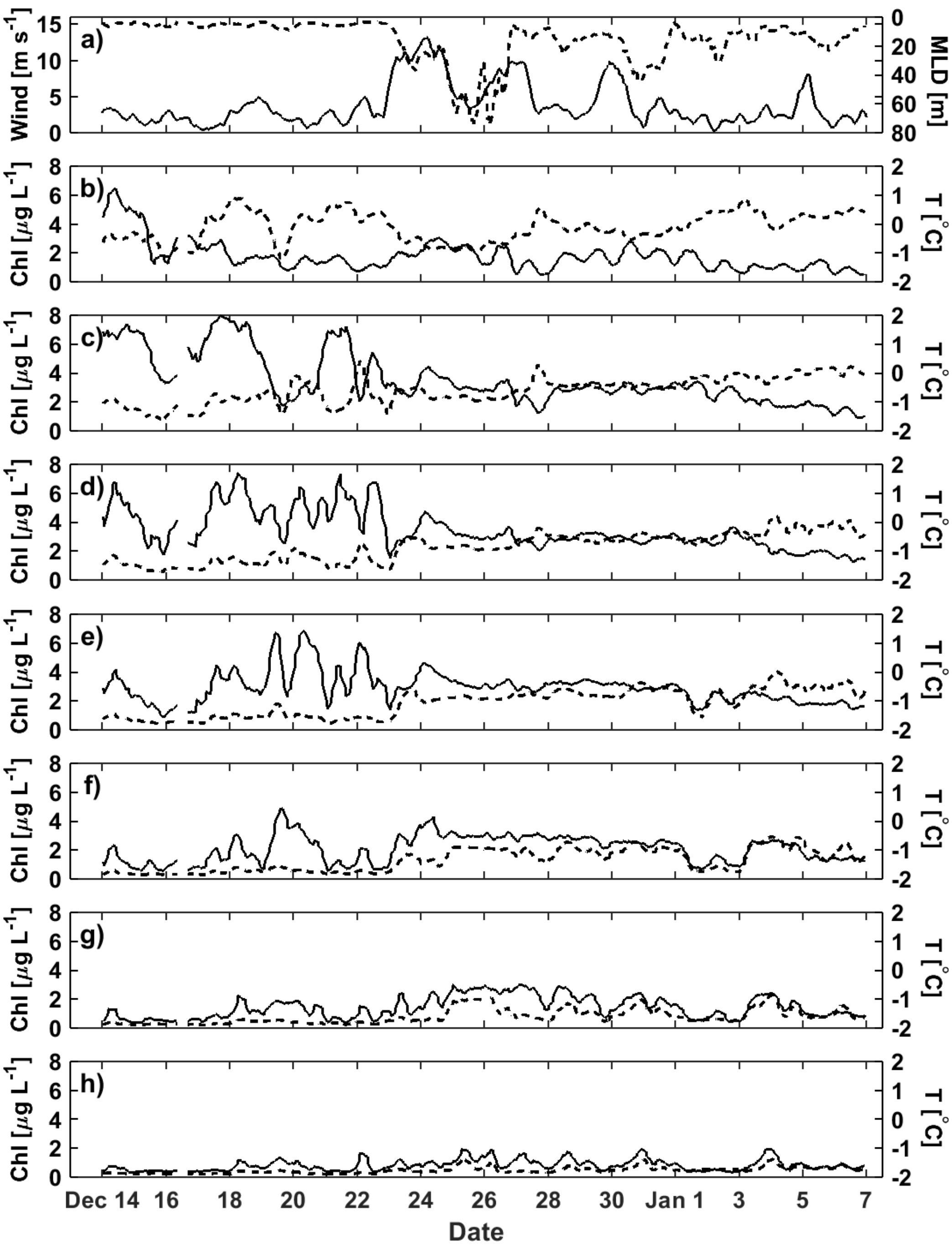
a)
b)
c)
d)
e)
f)
g)
h)
Wind [m s-1]
MLD [m]
Chl [μg L-1]
T [°C]
Dec 14
16
18
20
22
24
26
28
30
Jan 1
3
5
7
Date

Fig. 6

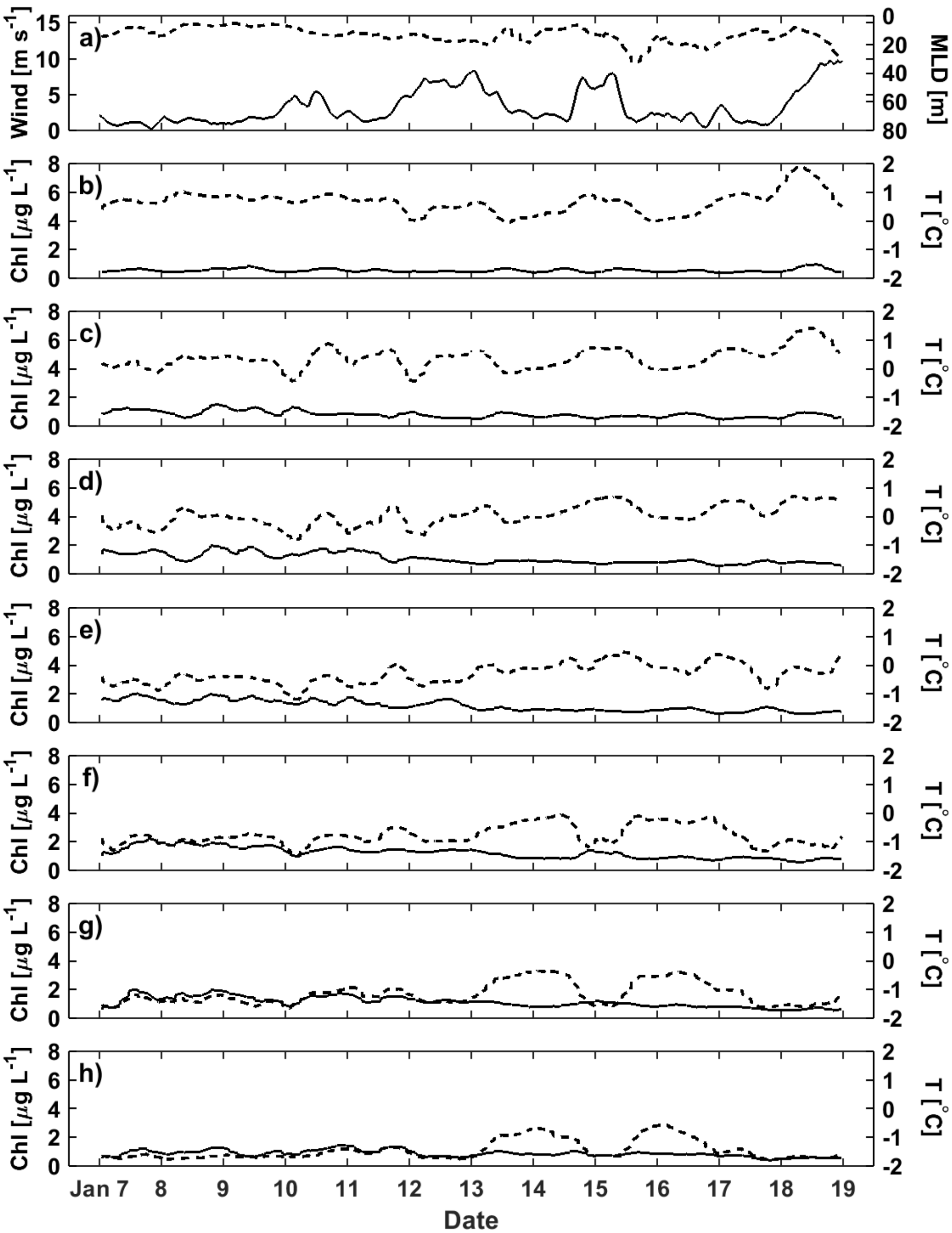
a)
b)
c)
d)
e)
f)
g)
h)
Wind [m s-1]
MLD [m]
Chl [μg L-1]
T [°C]
Jan 7
8
9
10
11
12
13
14
15
16
17
18
19
Date

Fig. 7

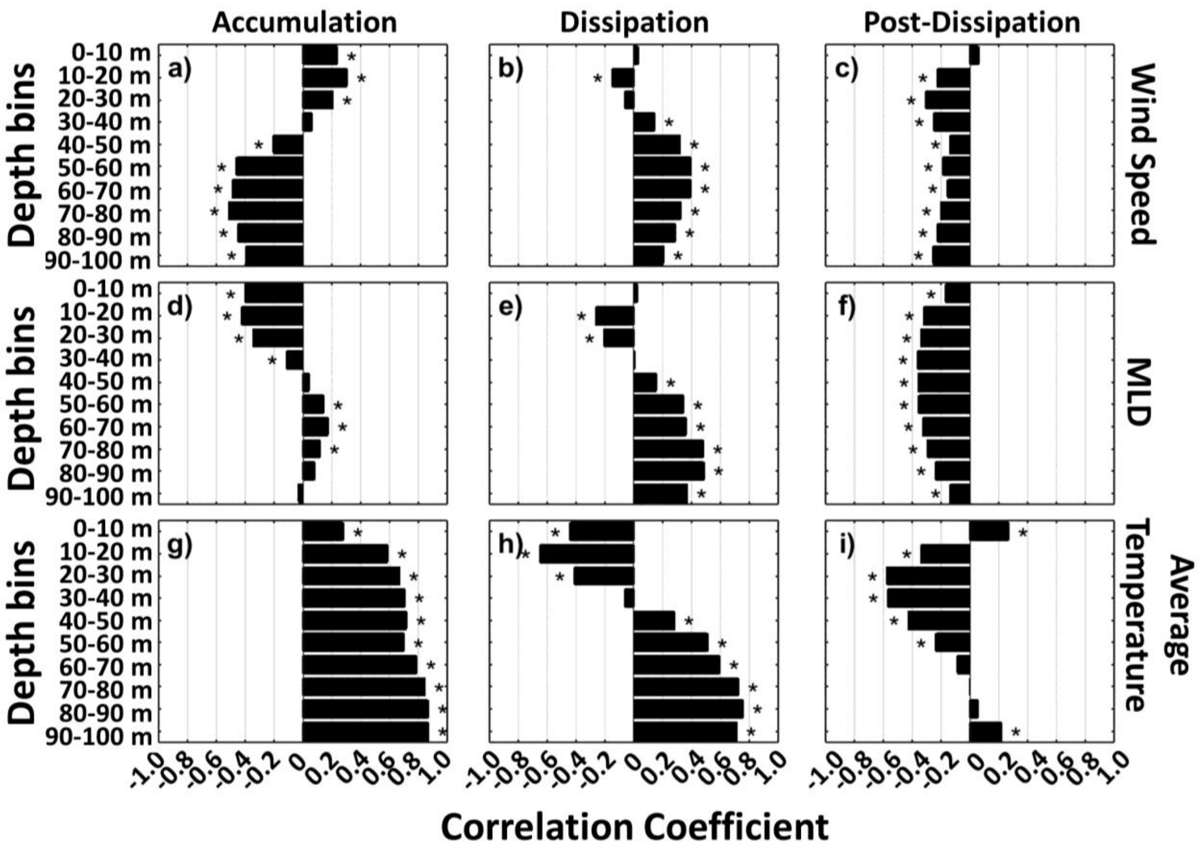
Accumulation
Dissipation
Post-Dissipation
Depth bins
0-10 m
10-20 m
20-30 m
30-40 m
40-50 m
50-60 m
60-70 m
70-80 m
80-90 m
90-100 m
a)
b)
c)
d)
e)
f)
g)
h)
i)
Wind Speed
MLD
Average Temperature
-1.0 -0.8 -0.6 -0.4 -0.2 0 0.2 0.4 0.6 0.8 1.0
Correlation Coefficient

704 Fig. 8

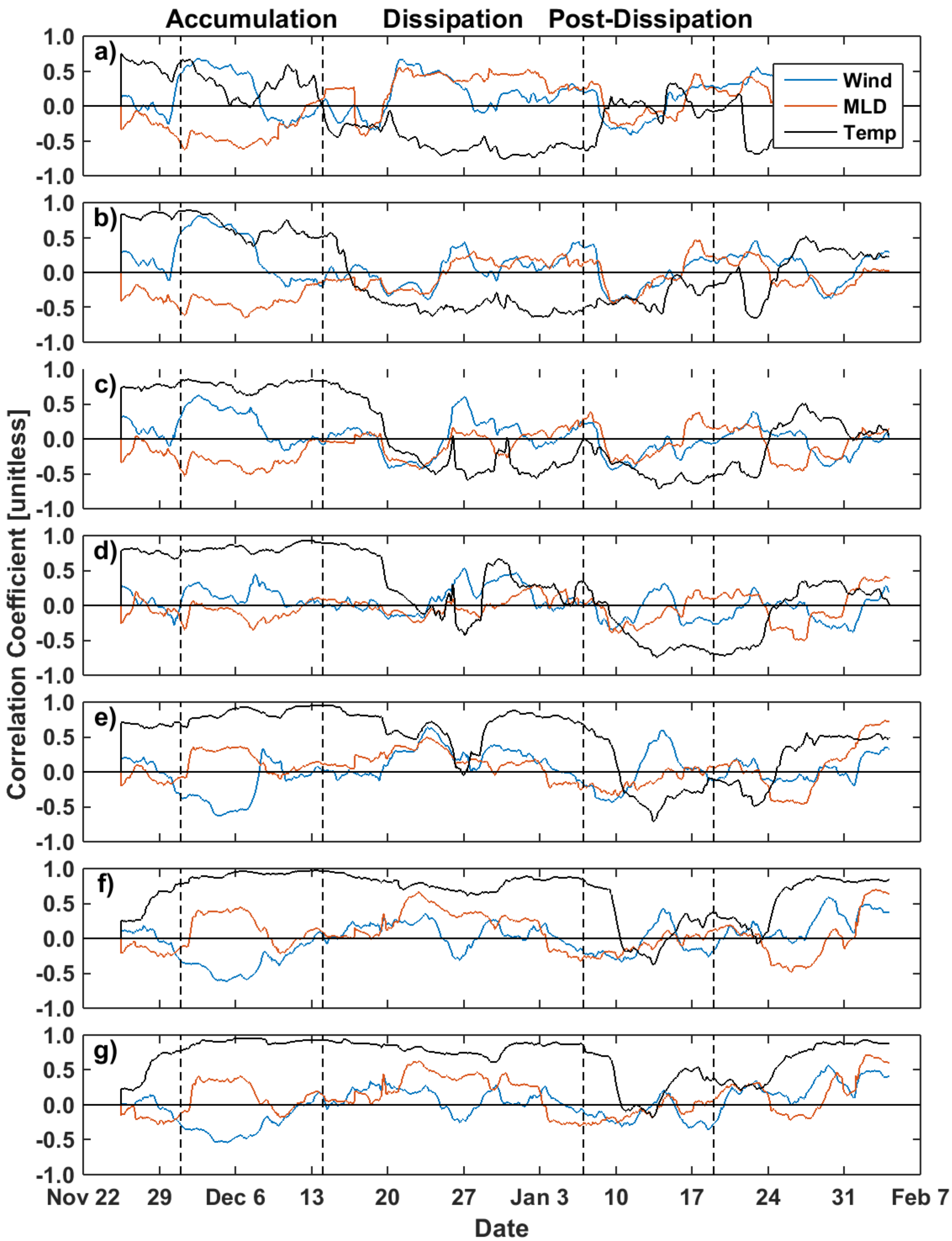
Accumulation
Dissipation
Post-Dissipation
a)
b)
c)
d)
e)
f)
g)
Wind
MLD
Temp
1.0
0.5
0.0
-0.5
-1.0
Correlation Coefficient [unitless]
Nov 22
29
Dec 6
13
20
27
Jan 3
10
17
24
31
Feb 7
Date

705